Dielectric response of vulcanized natural rubber containing $BaTiO_3$ filler: The role of particle functionalization

Neudys González[1,2], Maria dels Àngels Custal[2], Georgia N. Tomara[3], Georgios C. Psarras[4,*], Jordi-Roger Riba[5], Elaine Armelin[1,6*]

[1]*Departament d'Enginyeria Química, Universitat Politècnica de Catalunya, Campus Diagonal Besòs (EEBE), C/ d'Eduard Maristany 10-14, Edifici I2, 08019, Barcelona, Spain.*

[2]*Sicame Company, C/ Zinc 14 – Polígono Industrial Aquiberia, 08755, Castellbisbal, Spain.*

[3]*Department of Physics, School of Natural Sciences, University of Patras, 26504, Patras, Greece.*

[4]*Department of Materials Science, School of Natural Sciences, University of Patras, 26504, Patras, Greece.*

[5]*Departament d'Enginyeria Elèctrica, Universitat Politècnica de Catalunya, C/ Colom 1, 08222, Terrassa, Spain.*

[6]*Barcelona Research Center in Multiscale Science and Engineering, Universitat Politècnica de Catalunya, Campus Diagonal Besòs (EEBE), C/ d'Eduard Maristany 10-14, Edifici IS, 08019, Barcelona, Spain.*

Corresponding authors: elaine.armelin@upc.edu and G.C.Psarras@upatras.gr

ABSTRACT

Natural rubber (NR) nanocomposites have been prepared with hydroxylated barium titanate filler ($BaTiO_3$-OH), employing emulsion polymerization followed by vulcanization process. The addition of barium titanate, a compound with high dielectric permittivity, was envisaged to increase the insulating properties of NR films, thereby reducing the electrical stress and the possibility of undesired arcing on their surfaces. The content of perovskite particles greatly affected both, the mechanical and the electrical properties, of the vulcanized films. It was observed that the optimum functionalized nanoparticle concentration is around 0.25-0.50 phr, range in which the elongation of break was maintained between 874-935 % and the tensile strength was between 4.40-4.80 MPa; whereas the dielectric permittivity (ε') is slightly lower than the pristine NR or the NR compounded with high content of $BaTiO_3$ nanoparticles. The dielectric study revealed the presence of two dielectric relaxation modes: (*i*) glass to rubber transition (α-relaxation) and (*ii*) interfacial polarization (IP), known as Maxwell−Wagner−Sillars (MWS) polarization. The comparison between small concentrations of non-functionalized and functionalized $BaTiO_3$ inside NR polymeric films lead to the conclusion that the dielectric breakdown strength is high for non-functionalized fillers, supposedly due to less IP polarization phenomena.

Keywords: Natural rubber, polymer composites, barium titanate, surface functionalization, dielectric spectroscopy.

1. Introduction

Thin electrically insulating elastomers are promising electromecanically active polymers to be used in sectors such as electrical generators, actuators, flexible capacitors, solar cells, batteries, strain sensors, electrical insulating devices, piezoelectric devices and others. However, there are not many techniques that can be employed for the electrical characterization of polymers. Their deformations, as for example under pressure inside probes using contact methods, can interfere to obtain accurate results.[1] The development of Broadband Dielectric Spectroscopy (BDS) technique,[2] during the mid-nineties, with extremely wide frequency range (from 10^{-6}Hz up to 10^{12}Hz) allowed the study of both molecular fluctuations and collective phenomena, phase transitions, charge and polarization effects in amorphous,[3-5] semi-crystalline,[6,7] and elastomeric polymer composites.[8-10] The versatility of dielectric spectroscopy allowed it to become a fundamental tool in multidisciplinary design, characterization, quality control and application of advanced functional materials and systems applied in such diverse fields.

Vulcanized natural rubber (NR) is a type of elastomer derived from latex, which is a colloidal suspension of micro sized rubber particles extracted from the *Hevea brasiliensis* tree and is widely used as a matrix resin to obtain green nanocomposites.[11,12] NR elastomer presents certain unique advantages over competitive synthetic rubbers in many applications caused by the unique combination of its physical-mechanical properties. Therefore, it has been used as dielectric elastomer transducers, protective thin films, adhesives, tires, gloves, coatings, joints, pipes, tubes, and others; and its applications are still growing. [13,14]

Nowadays, composites comprising a polymer matrix and ferroelectric ceramic with high dielectric constant filler (also called high-k composite materials) have been extensively explored to serve as dielectric materials in high-energy-density devices.[15,16] For several years, the nanoscale dispersion of inorganic particles in a polymeric matrix has been very convenient due to the positive reinforcing effect and specific properties that can generate these particles when they are finely dispersed in the polymer chains.[17,18] For instance, Dang *et al.* [19] have reported a review on the effect of nanosized materials to increase the permittivity of advanced materials, used in power-energy-storage devices. They stated, for example, that the dielectric permittivity decreases dramatically from 5000 to hundreds as the grain size of barium titanate ($BaTiO_3$) is reduced from 1 μm to 30 nm. This decrease is assigned to the reduction of the portion of polar tetragonal phase and the increase of the non-polar cubic one, due to the diminution of the particle size [19].

Among the ferroelectric ceramics barium titanate has been extensively investigated due to its high dielectric constant.[20-22] The $BaTiO_3$ crystal is a multifunctional oxide that exhibits complex phase transition, between 120 ºC and 1457 ºC it has a cubic perovskite structure that consists of corner linked oxygen octahedral containing $Ti^{4+,}$ with Ba^{2+}.[22] However, the ferroelectric ceramics usually have poor compatibility with the polymer matrices. They are very prone to agglomeration due to their high surface energy, especially when the concentration of the ceramic nanofillers is high, so it leads to percolative pathways through aggregated fillers, thus increasing the leakage current and hence lowering the dielectric breakdown strength of the nanocomposites.[24,25] To overcome this problem, surface functionalization is currently being employed.[26-28] By modifying the inorganic filler surface by chemical processes such as hydroxylation, amination, sulfonation and grafting polymers, the $BaTiO_3$ particles becomes more uniformly dispersed in a suitable solvent media, that in turn increases the overall dielectric constant, and the breakdown field strength of the polymer-ceramic composites.[29-31] Nevertheless, the interfacial dipole layer emerged by chemical modification of the surface by polar species, like $BaTiO_3$ hydroxylated particles, may play an important role on the electrical response of the polymer.[32]

A key aim of the present work is to study the dielectric permittivity of vulcanized NR polymers after adding very low concentrations of hydroxylated barium titanate ($BaTiO_3$-OH) nanoparticles, while retaining their other excellent physical properties. The novelty of the present work relies on the comparison of the interfacial interaction between non-functionalized and functionalized $BaTiO_3$ nanoparticles with the organic polymer matrix and its influence on its breakdown strength (E_B).

2. EXPERIMENTAL SECTION

2.1. Materials

All samples were prepared by employing commercially available reagents. Barium titanate nanopowder ($BaTiO_3$, particle size about 100 nm, according to the supplier), zinc oxide (ZnO), titanium dioxide (TiO_2) and hydrogen peroxide solution (H_2O_2) were supplied by Sigma Aldrich Spain. Sulfur (reagent grade) and zinc dibuthyl dithiocarbamate (ZDBC) were used as vulcanizing agent and accelerator, respectively. Cab-o-Sperse® (Cabot Corporation) was used as dispersant agent to incorporate $BaTiO_3$ functionalized particles to rubber formulation. The latex used in this study is a colloidal suspension doubly centrifuged to increase the rubber particles concentration. It was purchased from several suppliers (from Malaysia and Brazil) and used as

received. Fillers and other ingredients used for the latex formulation were also of commercial grade.

2.2. Surface hydroxylation of $BaTiO_3$ nanoparticles and preparation of NR/$BaTiO_3$-OH nanocomposites

The surface hydroxylation of $BaTiO_3$ nanoparticles with H_2O_2 was performed according to previous work reported by Jiang and co-workers.[33] Briefly, about 10 g $BaTiO_3$ nanoparticles and 80 mL aqueous solution of H_2O_2 (30 wt. %) were added to a round bottom flask and the mixture was sonicated for 10 min (8 second pulses at 50% of amplitude) and refluxed at 105 ºC for 24 h. Then the nanoparticles were recovered by centrifugation at 10000 rpm for 10 min and were washed with deionized water twice. Finally, the product was dried under reduced pressure at 80 ºC for at least 24 h until a constant weight was obtained.

The NR/$BaTiO_3$ nanocomposites were prepared with loadings in the range from 0.25 to 10 phr at 23 °C using a Heidolph mechanical overhead stirrer model (RZR-1) provided with radial flow impeller stirrer blade, with a rotor speed of 60 rpm. The compounding formulations used for the preparation of NR/$BaTiO_3$ nanocomposites are shown in Table 1. Once functionalized, barium titanate NPs (500 mg) were dispersed in 3 mL of Cab-o-Sperse® solution (Scheme 1, solution 1) with vigorous stirring and further sonicated for 20 min (8 second pulses at 50% of amplitude) using Sonopuls Ultrasonic Homogenizers (Bandelin, model HD 2200), to obtain a homogenous dispersion. The solution 2 in Scheme 1 corresponds to the preparation of the polymer emulsion. In this case, the solution of rubber was first mechanically stirred for 5 min, and then ZnO and TiO_2 were added and mixed for 2 min. Solution 1 was poured to solution 2 and ZDBC and sulfur were added stepwise and similarly stirred for 2 min. The emulsion was then further stirred for 30 min with mechanical stirring for complete homogenization. The rubber compound was finally poured onto Petri dishes to obtain films 1mm thick for the electrical studies. The Petri dishes were left to pre-vulcanize at 75 ºC for 2 h in an oven for obtaining the solid film. Afterwards samples were washed gradually in a bath with distilled water from 25 to 70 ºC, dried on air and then left to complete curing at 75 ºC for 24 h before testing. It is important to highlight that all solids were sonicated and dispersed on aqueous solutions before addition to the rubber emulsion (solution 2).

2.3. Physical-chemistry characterization

Infrared spectra were measured in the range of 600−4000 cm^{-1} with a FTIR 4100 Jasco spectrophotometer coupled to an attenuated total reflection (ATR) accessory with a diamond

crystal (Specac model MKII Golden Gate Heated Single Reflection Diamond ATR). Calorimetric data were obtained by differential scanning calorimetry (DSC) with a TA Instruments Q100 series equipped with a refrigerated cooling system (RCS). Experiments were conducted under a flow of dry nitrogen and with 8 mg of weight per sample. Heating and cooling runs were carried out at rates of 10 °C/min and operating at temperatures from -90 ºC to 200 ºC. Thermogravimetric analysis (TGA) was carried out with a Q50 thermogravimetric analyzer of TA Instruments at a heating rate of 10 ºC/min under nitrogen atmosphere from 30 ºC to 600 ºC. Inspection of the cryo-fractured surfaces of NR films was conducted by scanning electron microscopy (SEM) using a Focus Ion Beam (FIB) Zeiss Neon 40 instrument (Carl Zeiss, Germany). Films were covered with conductive carbon coating, by using a Mitec K950 Sputter Coater, before SEM analyses. SmartTiff software from Carl Zeiss SMT Ltd. was employed to measure the diameter of sonicated solid particles inside vulcanized rubber matrix. X-ray diffraction patterns were registered with a Bruker D8 Advance diffractometer, using CuKα radiation (λ=0.15406nm), equipped with One-dimensional LynxEye Detector. Rubber dishes of 15 mm of diameter and 1 mm of height were employed. Contact angle measurements were performed by employing OCA 20 (DataPhysics Instruments GmbH, Filderstadt) equipment and using the sessile drop method at room temperature. For the static contact angle (sCA) measurements, 1 μL droplets of distillated water were dispensed on the respective surfaces. The contact angle values (software SCA 20) were obtained as the average of ten independent measures for each sample. The stress–strain behavior of the vulcanized material was studied using a universal tensile testing machine (MTS, model 853, brand Instruments J. Bot. S.A. and Estaw32 software) at a speed rate of 500 mm/min and an initial gage length of 20 mm, using a load cell of 10 N according to the standard UNE-EN 60903. The tensile strength and elongation at break were then determined based on the stress–strain curves. Dynamic light scattering (DLS) NanoBrook Omni Zeta Potential Analyzer (from Brookheaven Instruments) was employed for particle size measurements using 10 mg/L of $BaTiO_3$ dilute aqueous solutions. The cross-link density (mol/cm^3) was determined by toluene swelling according to the ASTM D3616 standard method.[34]

2.4. Broadband dielectric spectroscopy (BDS) and ac dielectric tests

Dielectric measurements of all samples were conducted by means of Broadband Dielectric Spectroscopy (BDS) in the frequency range of 0.1 Hz to 1 MHz using an Alpha-N Frequency Response Analyzer, supplied by Novocontrol Technologies. Temperature was controlled via Quattro system, supplied also by Novocontrol Technologies, within the range 173.15 K (-100

ºC) to 423.15 K (150 ºC) with accuracy ±0.1 K. Isothermal frequency scans were performed for each of the examined specimens in steps of 10 K, whereas isothermal time for each temperature step was 4.5 minutes . The applied Vrms voltage was kept constant at 1.0 V and the employed dielectric cell was the BDS-1200 (Novocontrol Technologies) parallel plate capacitor with two gold-plated electrodes. Dielectric cell was suitable shielded in order to avoid any electromagnetic interference and data acquisition was conducted, in real time, with Windata software (Novocontrol Technologies). Samples were cut into circular disk form with diameter 24 mm and average thickness 1.0 mm. The diameter of the applied gold electrodes was 20 mm for the upper one and 30 mm for the lower one. This arrangement is suitable for avoiding the influence of any stray capacitance.

A Phenix BK130/36 variable high-voltage transformer was used to carry out the ac dielectric tests to determine the characteristic breakdown strength. The equipment allows selecting two output voltage ratings, that is, 0-36 kV and 0-130 kV. The Phenix BK130/36 includes precision voltage and current metering to fulfil the requirements of both the ASTM D120 [35] and IEC-60903 [36] standards. These experiments were performed according to the setup described on reference [12]. In order to get reproducible results, six breakdown tests were performed on each type of composite. Since the thickness of the tested latex samples is slightly different for each molded specimen, both leakage current and measured voltage were normalized with respect to their thicknesses.

3. RESULTS AND DISCUSSION

3.1. Evaluation of the presence of $BaTiO_3$-OH on NR films

The perovskite functionalization with hydrogen peroxide (H_2O_2) was followed by FTIR and the effectiveness of the hydroxylation reaction was previously reported on our recent work.[37] The presence of $BaTiO_3$-OH nanoparticles on the structure of NR films was also evaluated by FTIR spectroscopy (Figure 1). The main absorption bands correspond to the polymer matrix (NR), which are at 3045 cm^{-1} (=CH stretching), 2963 cm^{-1} (C−H stretching of CH_3), 2856 cm^{-1} (C−H stretching of CH_2 and CH_3), 1664 cm^{-1} (C=C stretching), 1449 cm^{-1} (C−H bending of CH_2), 1376 cm^{-1} (C−H bending of CH3), and 837 cm^{-1} (C=CH wagging) (Figure 1a). In Figure 1b, it was also observed that the absorption bands at 1447 cm^{-1} and 1000 cm^{-1} increased with the high content of filler load, since they are related to the residual barium

carbonate ($BaCO_3$) compound usually observed in $BaTiO_3$ NPs,[38,28] and the -OH bending vibrations of functionalized $BaTiO_3$ particles, respectively.[37]

Additionally to FTIR analysis, XRD has been demonstrated that perovskite ceramic particles were successfully incorporated to the polymer matrix (Figure 2). The diffraction model shows that $BaTiO_3$-OH functionalized has very sharp peaks, thus indicating a crystalline structure, whereas unmodified NR has a broad peak between 10º and 30º, indicating mostly amorphous phase. The main characteristic reflections of $BaTiO_3$-OH on X-ray diffraction can be observed at 21.5º, 31.5º, 38.9º, 45.5º, 50.9º, 56.1º, 66.1º, 40.5º and 75.1º (2θ), which are related to (100), (110), (111), (200), (210), (211), (220), (300) and (310) lattice planes, respectively.[39] In the case of NR/$BaTiO_3$-OH nanocomposites the peaks from these ceramic particles appeared indeed at very low concentration of filler (NR/$BaTiO_3$-OH 0.25 phr). With increased filler content some new and more intense peaks corresponding to this ceramic compound appeared in the polymer diffractogram, showing that the vulcanized NR was well compounded.

3.2. Influence of the $BaTiO_3$-OH content on the thermal, morphology and mechanical properties of NR films

Pristine NR and NR/$BaTiO_3$-OH nanocomposites were analyzed by DSC (Figure 3a) and TGA (Figure 3b) to obtain their glass transition temperatures (T_g) and thermal stability, respectively. Low effect of the filler particles on the calorimetric glass transition of NR films was observed in terms of shifting or broadening, as can be seen on Figure 3a and in Table 2. However, the low filler content used in the present work caused a better nanoparticle dispersion on the rubber emulsion since it displayed improved cured films (as observed by the swelling index, see results below) compared to other works, where high content of inorganic nanoparticles are present. One example is the research recently reported by M. Huang *et al.* [40]. They performed a complete study (employing complementary techniques like DSC, BDS and DMA) on the relaxation processes of NR films compounded with very high concentration of carbon black and silica nanoparticles (50 phr to 100 g of rubber). They attributed the scarce evidences for the influence of filler particles on the T_g of the bulk polymer, or in the polymer relaxation times of the filled rubbers, to the nature of polymer confinement related to the imperfect dispersion state of the nanoparticles. However, other studies shown a slight alteration of the polymer's T_g, in filled elastomers and thermoplastics, when non-agglomerated nanoparticles are present.[24,41,42] This phenomena can be explained by the effect of restriction of chain movement caused by an increase on the cross-linking degree.

Figure 3b shows a typical TGA analysis of a NR elastomer. The TGA curve exhibits two steps. The first step below about 300 ºC of weight loss of 3.1% (only appreciated with the derivative curve, data not shown), corresponds to the loss of small quantities of relatively volatile components. Pyrolysis of the elastomer takes place between 300-550 ºC. Therefore, the second step corresponds to a polymer content of about 63% for all cases. The unique variation observed with the increase $BaTiO_3$ filler content was in the char yield (Figure 3b, inset). The material residue increased from 1.8 to 9.99 wt. % with loadings from 0.25 to 10 phr of $BaTiO_3$-OH. The presence of $BaTiO_3$ could probably increase the char residue due the formation of oxides which decomposes higher than 600 ºC. The TGA shows that vulcanized NR starts to decompose at around 250 ºC and steadily decomposed at 450 ºC. All DSC and TGA results are presented in Table 2.

The $BaTiO_3$ functionalization with H_2O_2 would promote a better interfacial dispersion of the ceramic particles on the NR polymer matrix. Before addition to the latex formulation, the particle size was checked with light scattering. It varied from 156 ± 41 nm for pure $BaTiO_3$ to 203 ± 80 nm for $BaTiO_3$-OH in aqueous solutions (S1, Supporting information). The nanosized dimension of the spherical particles was maintained thanks to the sonication process (Scheme 1). Therefore, the morphology of cross-sectional area revealed the presence of well dispersed $BaTiO_3$ ceramic compound when the content was not higher than 5 phr (Figure 4), showing a good dispersion with the latex emulsion. For example, the polydispersity varied from 4% to 42% for NR/$BaTiO_3$-OH 0.5 phr and NR/$BaTiO_3$-OH 10 phr, respectively, evidencing some tendency to agglomeration when the filler content was high. It also will have consequences on the electrical behavior of the solid films, as will be discussed below. Thus, the agglomerates size varied from 3.0 ± 0.1 μm to 4.3 ± 1.8 μm for NR/$BaTiO_3$-OH 0.5 phr and NR/$BaTiO_3$-OH 10 phr, respectively, after rubber vulcanization, measured with the SmartTiff software of FIB microscope. It is probably due to the electrostatic interaction among $BaTiO_3$ and the other ceramic fillers, like ZnO and TiO_2 also present in the rubber formulation. Repulsion forces generate interfacial interaction between the particles. This kind of interaction caused agglomeration of these particles, but also, generated interaction with the polymer matrix, as can be seen by SEM images. The individual particle size of solid substance inside these agglomerates varied from 74.0 ± 17.7 nm and 124.3 ± 15.5 nm for 0.5 phr and 10 phr, respectively.

As the $BaTiO_3$ was added in low concentrations and was in general satisfactory distributed, it only appeared in the EDX analysis (Figure 4m) when the content was close to 10

phr, as can be seen by the spectrum taken from the white particles observed on the Figures 4k and 4l. Due to the presence of other fillers, like ZnO and TiO_2, necessary for the latex formulation, the nanosized dimension of $BaTiO_3$ added at the beginning changed to a more agglomerated system after the vulcanization process. Nevertheless, other properties revealed it does not have a negative effect on the polymer performance; on the contrary, there are some properties that have been enhanced, as will be discussed later.

On the other hand, the volume fraction of rubber is an important parameter that can be taken as a measure of the cross-link density of the polymer. The mechanical properties of elastomers will be strongly affected by this property. The quantitative determination of the cross-link degree is always difficult for filled rubber due to the distinct nature of cross-linker agents and accelerators [43] indeed will be affected by the natural cross-link linkages usually found in latex [44].

According to the ASTM D3616,[34] the degree of swelling is an qualitative indication of effectiveness of the curing process and can be measured by the equation (1):

$$Swelling \cdot index = \frac{W_2 - W_1}{W_1} \qquad (1)$$

where W_1 is the initial mass of dry solid film and W_2 is the mass of wet solid film after swelling in toluene.

The swelling study demonstrated that all systems are satisfactory crosslinked even if the ceramic content are high (values among 5-7), however the NR/$BaTiO_3$-OH 0.25 phr and 0.50 phr are completely vulcanized with the lowest swelling degree (< 5, Figure S2), which is corroborated by their better mechanical properties (elongation at break and tensile strength).

As can be seen in the Figure 5, the tensile strength decreased after $BaTiO_3$ concentration higher than 1 phr. The same observation is applied for the elongation at break despite it is high enough for this kind of polymer and supposedly will not affect their performance. Nevertheless, the stress-strain experiment gives us an idea about the percolation threshold for perovskite addition to the elastomer matrix. Due to the presence of mainly non-polar groups, C=C and C-H linkages, on natural rubber polymer the interaction of surface hydroxylated $BaTiO_3$, mostly polar, with the organic molecules played a contrary effect than we would expect. Increased filler concentrations were traduced in low chain interactions and high agglomeration probability. Kargarzadeh *et al.* [45] recently discussed the compatibility and polarity effect of an epoxydized

NR on the mechanical properties of a polyester resin. The oxyrane rings act as active centres in the liquid rubber polyisoprene for the adhesion interaction with the unsaturated polyester chains. To conclude, the compounding fabrication of NR films with polar inorganic fillers is not an easy task and several parameters will affect the good compatibility among reagents.

3.3. Influence of the $BaTiO_3$-OH content on the dielectric properties of NR films

It is well known that high dielectric permittivity is usually achieved by adding high volume fraction of inorganic particles. However, it undoubtedly results in a sharp decrease of the dielectric breakdown strength, as the density of cracks and void defects increases.[46,47] Recent studies show that some composites with enhanced dielectric permittivity can be obtained by enlarging the interfacial areas as a result of promoting the polarization between the ceramic-polymer matrix interfaces.[5,48,49] Choosing an appropriate content and particle size are both critical approaches to optimize the dielectric compatibility. With the nanofillers the interfacial area between inorganic particles and polymer matrix is enhanced, compared to microsized composites, creating an adequate volume fraction. Moreover, it will affect the thermal and dielectric responses of the composites from particle-polymer and particle-particle interactions.

The experiments in this study were conducted from 173.15 K (-100 ºC) to 423.15 K (+150 ºC), the range in which the elastomer does not degrade. Therefore, two relaxation processes were detected in the dielectric spectra, namely α-relaxation or segmental mode (SM) and interfacial polarization (IP), known as Maxwell−Wagner−Sillars (MWS) polarization. The first phenomenon is derived from glass to rubber transition of the elastomer matrix, *i.e.* the dynamic glass transition; that occurs at about 213.15-203.15 K (-60 to -70 ºC); whereas the latter appears at high temperature and low frequency and is attributed to the charge accumulation in the particle-polymer interface. López-Manchado and co-workers [10] extensively studied the molecular dynamics of non-vulcanized and vulcanized NR and NR/layered silicates nanocomposites by means of dielectric spectroscopy. They determined the presence of two dielectric relaxation modes in non-vulcanized NR: (*i*) the segmental mode (SM), attributed to the segmental motions of the polymer chains (α-relaxation), and (*ii*) the normal mode (NM) associated with the dynamics of the whole chain.[50,51] The latter is characterized by the end-to-end dipole vector, which results as the summation of the molecular dipole vectors of the repeat units.[52] In the case of vulcanized NR and its associated nanocomposites they reported the absence of NM phenomena, since the corresponding relaxation loss peak becomes broader and diminishes in amplitude due to the limited motion of dipoles parallel to the main polymer chain. In addition, they observed another slow dielectric relaxation process, which was attributed to IP.[10]

In the present study, the dielectric response becomes stronger for the composite with low concentration of $BaTiO_3$-OH particles, *i.e.* with the composition of 0.25 phr and 0.50 phr. It is supposedly attributed to the better dispersion of the low concentration functionalized ceramic particles within the rubber matrix, as proved by SEM, which also favoured a better cross-linking process, proved by swelling measurements. It was also observed by Xu *et al.* [53] with thermoplastic polymers, poly(vinylidene fluoride-co-hexafluoropylene) [P(VDF-HFP)], modified with flower-like TiO_2 filler. A similar behavior has been reported by Q. Huang *et al.* [54], who described that the interfacial polarization of P(VDF-HFP) nanocomposites fabricated with TiO_2/$BaTiO_3$ fillers, kept a relatively stable value, especially when the content of the fillers was lower than 10 vol. %.

An advantage of the present work is that ceramic nanoparticles were sonicated prior being incorporated in the NR formulation for further vulcanization, instead of directly dispersed in a polymer matrix. Thus, the insulating polymer shell around the nanoparticles is found to be capable of serving as an effective barrier, retarding the movement of charge carriers in the NR composites. Figure 6a presents the variation of the real part of dielectric permittivity (ε′) as a function of frequency at 253.15 K (-20 ^oC), for all the examined systems. Permittivity decreases with frequency, as expected, reflecting the levelling off of polarization, since dipoles fail to follow the rapid alternation of the field. This behavior is more pronounced at higher temperatures (see Figures S3-S8). Although, the dielectric permittivity of the filler is much higher than that of the matrix, nanocomposites with low filler content exhibit lower values of ε′ with respect to pure NR. As already noted, ε′ is proportional to polarization and it is the result of the orientation of molecular and/or macromolecular dipoles parallel to the field, since at this low temperature the slow process of interfacial polarization has not come into play and thus can be neglected.

Therefore, at low filler content, nanoparticles are apart from each other, and thus the particle-particle interactions appear to be neglected compared to the particle-macromolecules interactions. The latter apply restrictions to the molecular and macromolecular mobility, causing a decrease of polarization and dielectric permittivity. Moreover, at the low concentrations of the reinforcing phase, the contribution of the high permittivity of barium titanate to the overall ε′ remains significantly low. As the filler content increases, the contribution of $BaTiO_3$-OH to the permittivity of nanocomposites enhances, thus switching the predominant interaction to particle-particle. By these means, restrictions to molecular mobility are, at least partially removed, thus easing dipoles orientation and resulting in higher values of the dielectric permittivity. At the highest filler content, the number of nanoparticles increases significantly, allowing both types of

interactions to augment, resulting in a small decrease of ε′. Figure 6b shows the spectra of the imaginary part of dielectric permittivity (ε″) as a function of frequency at 253.15 K (-20 ^{o}C), for all systems. The dielectric loss peaks correspond to glass to rubber transition of NR (α-relaxation) and the position of their maxima varies slightly with the filler concentration. At the low frequency region, some experimental noise has been also recorded.

On the other hand, IP was also observed, derived from the nanoceramic/polymer interfaces present on polymer matrix. It is better seen by plotting the dielectric permittivity (ε′) versus temperature at a constant frequency (Figure 7). This phenomenon is attributed to the accumulation of unbounded charges at the interface between the matrix and filler, where they form large dipoles. These dipoles exhibit enhanced inertia in being oriented parallel to the applied field, and thus the IP-process is characterized by high relaxation times and recorded in high-temperature and low-frequency region. IP is usually present in composites and heterogeneous systems consisted of materials with different electrical characteristics, like that employed here. As can be seen on the Figure 7a, at temperatures below 223.15 K (-50ºC), a small step-like increase of ε′ is present in the spectra of all specimens. This increment is the result of the enhanced segmental mobility achieved in the vicinity of T_g, or above it, and is assigned to the α-relaxation phenomenon. At high temperatures, a more intense increase of ε′ is observed, implying the presence of the IP phenomena.

Dielectric data can be expressed in different formalisms, *i.e.* dielectric permittivity, electric modulus and ac conductivity. All three formalisms describe the same relaxation phenomena, although under various conditions a specific formalism could be proved more efficient in extracting information for occurring physical processes.[55] The electric modulus is defined as:

$$M^* = \frac{1}{\varepsilon^*} = \frac{1}{\varepsilon' - i\varepsilon''} = \frac{\varepsilon'}{\varepsilon'^2+\varepsilon''^2} + i\frac{\varepsilon''}{\varepsilon'^2+\varepsilon''^2} = M' + iM'' \qquad (2)$$

where M' and M'' are the real and imaginary parts of the electric modulus. The advantages of describing the dielectric data via the electric modulus formalism are presented elsewhere.[10,55]

Additionally, to the variation of the dielectric permittivity (ε′), the loss modulus index (M'') was also depicted on Figure 7b. The formation of two loss peaks is evident. The first one, recorded in the vicinity of 213.15 K (-60ºC), corresponds to the SM-mode (α-relaxation), and its position is related to the glass transition temperatures of the samples. The second one, recorded at high temperatures, denotes the IP process. Inset of Figure 7b, presents IP loss peak as a function

of frequency at 423.15 K (150 ºC). In general, the relaxation peak of nanocomposites tends to be formed at lower frequencies with respect to the peak of NR. Shifting relaxation peaks to lower frequencies imply slower processes with longer relaxation times. NR contains ingredients which are responsible for the occurrence of IP, as mentioned before. However, the existence of barium titanate/NR interfaces and the interactions at the interface zone, slow down the IP-process, shifting the peaks to lower frequencies.

All the BDS plots for each sample of different formalisms such as dielectric permittivity, dielectric modulus and dielectric loss, are also shown in the Supporting Information.

3.4. Comparison of electric breakdown strength between functionalized and non-functionalized $BaTiO_3$ content inside vulcanized NR

AC dielectric tests were also performed in order to check the characteristic breakdown strength of NR films with thickness of about 1 mm. It is well known that the energy density (U_e) is determined by the applied electric field (E) and the electric displacement (D) of the dielectric, according to the eq. (3):

$$U_e = \int_{D_{\max}}^{0} E dD \qquad (3)$$

where D_{max} is the electric displacement at the highest field, E is the applied electric field and D is electric displacement also called electric flux density. For linear dielectric materials, such as polymers and their composites, eq. (3) can be expressed as:

$$U_e = \frac{1}{2} DE = \frac{1}{2} \varepsilon_0 \varepsilon_r E^2 \qquad (4)$$

where ε_r and ε_0 (8.85×10^{-12} F/m) are the dimensionless relative permittivity and the vacuum permittivity, respectively. Therefore, the energy density is proportional to the relative permittivity and square of the electric field, which is limited by the dielectric breakdown strength (E_b).[22] The relative permittivity (ε_r) and the breakdown strength (E_B) are of significant importance. The energy density (U_e) is largely determined by E_B.[56,57]

The characteristic breakdown strengths of pristine NR and NR/$BaTiO_3$-OH nanocomposites are illustrated in Figure 8 and compared to our previous work with non-functionalized $BaTiO_3$ particles.[12] All of the NR/$BaTiO_3$ composites could withstand a high electric field over 18-20 kV/mm and 23-25 kV/mm, for hydroxylated and non-functionalized $BaTiO_3$ nanoparticles, in ac dielectric tests, respectively; if the filler content is very low. The breakdown strength increases with the increase of the loading volume fraction (> 0.5 phr), as a result of the agglomeration and voids created inside the polymer chains due to the worse particle

dispersion, and therefore the breakdown strength decreases to values similar to those of pristine NR (13.2 ± 1.2 kV/mm). Thus, it can be stated that the percolation threshold for NR nanocomposite fabrication employing this kind of perovskite particles, either functionalized or non-functionalized, would be between 0.40 and 0.50 phr.

Aforementioned results indicate that NR/$BaTiO_3$ (non-functionalized) composites show much greater E_B than the hydroxylated $BaTiO_3$ counterparts. Therefore, the NR/$BaTiO_3$ composites with pristine perovskite nanoparticles seem to exhibit the enhanced electrical properties for manufacturing insulating devices over the hydroxylated-$BaTiO_3$ system. The electrical behavior of NR/$BaTiO_3$-OH in dc polarization tests (positive and negative polarity) is reported elsewhere [37].

4. CONCLUSIONS

Usually, the scientific community is rather interested on search for high permittivity elastomer composites by pursuing it with different conductive fillers, like carbon nanotubes, graphene, carbon black micro-particles, metal particles, and others. By contrary, in this project we were interested on achieve low electric permittivity to obtain a high insulating performance. Then, an extensive study evaluating and comparing the effect of the nanofiller content on thermal, mechanical and electrical properties of NR films was carried out. The influence of the perovskite functionalization revealed that high concentrations (> 5 phr) of this kind of ceramic particles are negative and are rather self-defecting, whereas low concentrations (among 0.25-0.50 phr) is beneficial.

The maximum breakdown strength was found for NR/$BaTiO_3$-OH with 0.50 phr content (18 kV/mm) compared to the pristine NR films (13 kV/mm). However, the best breakdown strength was achieved for non-functionalized ceramic particle-NR nanocomposites, which were 25 kV/mm for either 0.40 phr or 0.50 phr of NR/$BaTiO_3$ films. These results were attributed to the existence of low concentration of barium titanate/NR interfaces, which contributed to decrease the permittivity of the nanocomposite. At low filler concentration the conductive particles are separated from each other and the electrical properties of the composites are still dominated by the matrix. As the concentration increases, the fillers start to form a three dimensional network through the matrix, giving rise to an increase in the electrical conductivity.

Therefore, to conclude, by working at concentrations below 0.50 phr of $BaTiO_3$ non-functionalized NPs it is possible to slightly increase the insulating properties of vulcanized NR

films, achieving low dielectric permittivity; and it is also possible to maintain the long elongation at break, *i.e.* taking advantage of the intrinsic properties of elastomers.

Acknowledgements

The present work has been supported by Generalitat de Catalunya (Spain) with the Industrial Doctorate programme. N. González acknowledges the fellowship (2013DI036) promoted by the Industrial Doctorate programme. This work has been also supported by interdisciplinary projects: MICINN and FEDER funds (MAT2015-69367-R) from Ministry of Education, Culture and Sport of Spain.

REFERENCES

[1] F. Carpi *et. al.* Standards for dielectric elastomer transducers, Smart Mat. Struct. 24 (2015) 105025-105051.

[2] F. Kremer, A. Schönhals, Broadband Dielectric Measurement Techniques: (10^{-6} Hz to 10^{12} Hz), in *Broadband Dielectric Spectroscopy*, F. Kremer, A. Schönhals (Eds.), Springer-Verlag Berlin Heidelberg 2003 Chapter 2, pp 35-57.

[3] A. Patsidis, G. C. Psarras, Dielectric behavior and functionality of polymer matrix-ceramic $BaTiO_3$ composites. Express Polym. Lett. 2 (2008) 718–726.

[4] I. A. Asimakopoulos, G. C. Psarras, L. Zoumpoulakis. Barium titanate/polyester resin nanocomposites:Development, structure-properties relationship and energy storage capability. Express Polym. Lett. 8 (2014) 692–707.

[5] O. Vryonis, D.L. Anastassopoulos, A.A. Vradis, G.C. Psarras. Dielectric response and molecular dynamics in epoxy-$BaSrTiO_3$ nanocomposites: Effect of nanofiller loading. Polymer 95 (2016) 82–90.

[6] Z-M. Dang, H-Y. Wang, Y-H. Zhang, J-Q. Qi, Morphology and Dielectric Property of Homogenous $BaTiO_3$/PVDF Nanocomposites Prepared via the Natural Adsorption Action of Nanosized $BaTiO_3$. Macrom. Rap. Comm. 26 (2005) 1185–1189.

[7] S. Dalle Vacche, F. Oliveira, Y. Leterrier, V. Michaud, D. Damjanovic, J-A. E. Manson, Effect of silane coupling agent on the morphology, structure, and properties of poly(vinylidene fluoride–trifluoroethylene)/BaTiO3 composites. J. Mat. Sci. 49 (2014) 4552–4564.

[8] S. Salaeh, G. Boiteux, P. Cassagnau, C. Nakason. Flexible 0-3 Ceramic-Polymer Composites of Barium Titanate and Epoxidized Natural Rubber. Int. J. Appl. Ceram. Technol. 12 (2015) 106–115.

[9] L. Jiang, A. Betts, D. Kennedy, S. Jerrams. Improving the electromechanical performance of dielectric elastomers using silicone rubber and dopamine coated barium titanate. Materials and Design 85 (2015) 733–742.

[10] M. Hernández, R. Verdejo, J. Carretero-González, T.A. Ezquerra, M.A. López-Manchado. Molecular Dynamics of Natural Rubber/Layered Silicate Nanocomposites As Studied by Dielectric Relaxation Spectroscopy. Macromolecules 43 (2010) 643–651.

[11] A. Ladhar, M. Arous, H. Kaddami, M. Raihane, A. Kallel, M. P. F. Graça, L. C. Costa. Ionic hopping conductivity in potential batteries separator based on natural rubber–nanocellulose green nanocomposites. J. Molec. Liquids, 211 (2015) 792–802.

[12] N. González, M. A. Custal, S. Lalaouna, J-R. Riba, E. Armelin. Improvement of dielectric properties of natural rubber by adding perovskite nanoparticles, Eur. Polym. J., 75 (2016) 210–222.

[13] N. Wang, L. Mi, Y. Wu, J. Zhang, Q. Fang. Double-layered co-microencapsulated ammonium polyphosphate and mesoporous MCM-41 in intumescent flame-retardant natural rubber composites. J. Therm. Anal. Calorim. 115 (2014) 1173–1181.

[14] M. Mariano, N. El Kissi, A. Dufresne. Cellulose nanocrystal reinforced oxidized natural rubber nanocomposites. Carbohyd. Polym. 137 (2016) 174–183.

[15] A. Choudhury. Preparation, characterization and dielectric properties of polyetherimide nanocomposites containing surface-functionalized $BaTiO_3$ nanoparticles Polym. Int. 61 (2012) 696–702.

[16] S. Wang, X. Huang, G. Wang, Y. Wang, J. He, P. Jiang. Increasing the Energy Efficiency and Breakdown Strength of High- Energy-Density Polymer Nanocomposites by Engineering the $Ba_{0.7}Sr_{0.3}TiO_3$ Nanowire Surface via Reversible Addition−Fragmentation Chain Transfer Polymerization. J. Phys. Chem. C 119 (2015) 25307−25318.

[17] X. Zhang, H. Chen, Y. Ma, C. Zhao, W. Yang. Preparation and dielectric properties of core–shell structural composites of poly(1H,1H,2H,2H-perfluorooctyl methacrylate)@$BaTiO_3$ nanoparticles. Appl. Surf. Sci. 277 (2013) 121−127.

[18] M. Valera, A. Yescas, E. Juarez, A. Aguirre, A. Aparicio, E. Ramírez, S. Sepúlveda, S. Sánchez. Immobilization of TiO_2 nanoparticles on montmorillonite clay and its effect on the morphology of natural rubber nanocomposites. Polym. Bull. 71 (2014) 1295–1313.

[19] Z-M. Dang, J-K. Yuan, S-H. Yao, R-J. Liao. Flexible Nanodielectric Materials with High Permittivity for Power Energy Storage. Adv. Mater. 25 (2013) 6334–6365.

[20] G. Garnweitner, J. Hentschel, M. Antonietti, M. Niederberger. Nonaqueous Synthesis of Amorphous Powder Precursors for Nanocrystalline $PbTiO_3$, $Pb(Zr,Ti)O_3$, and $PbZrO_3$. Chem. Mater. 17 (2005) 4594–4599.

[21] B. Luo, X. Wang, Q. Zhao, L. Li. Synthesis, characterization and dielectric properties of surface functionalized ferroelectric ceramic/epoxy resin composites with high dielectric permittivity. Compos. Sci. Tech. 112 (2015) 1–7.

[22] X. Su, B. C. Riggs, M. Tomozawa, J. K. Nelson, D. B. Chrisey. Preparation of $BaTiO_3$/low melting glass core–shell nanoparticles for energy storage capacitor applications. J. Mater. Chem. A, 2 (2014) 18087–18096.

[23] P. Ctibor, H. Ageorges, V. Stengl, N. Murafa, I. Pis, T. Zahoranova, V. Nehasil, Z. Pala. Structure and properties of plasma sprayed $BaTiO_3$ coatings: Spray parameters versus structure and photocatalytic activity. Ceram. Intern. 37 (2011) 2561–2567.

[24] H. Tang, P. Wang, P. Zheng, X. Liu. Core-shell structured $BaTiO_3$@polymer hybrid nanofiller for poly(arylene ether nitrile) nanocomposites with enhanced dielectric properties and high thermal stability. Compos. Sci. Tech. 123 (2016) 134–142.

[25] T. Tanaka. Dielectric nanocomposites with insulating properties, IEEE Trans. Dielectr. Electr. Insul, 12 (2005) 914–928.

[26] M. N. Almadhoun, U. S. Bhansali, H. N. Alshareef. Nanocomposites of ferroelectric polymers with surface-hydroxylated $BaTiO_3$ nanoparticles for energy storage applications. J. Mater. Chem., 22 (2012) 11196–11200.

[27] S-J. Chang, W-S. Liao, C-J. Ciou, J-T. Lee, C-C. Li. An efficient approach to derive hydroxyl groups on the surface of barium titanate nanoparticles to improve its chemical modification ability. J. Coll. Interf. Sci. 329 (2009) 300–305.

[28] C-C. Li, S-J. Chang, J-T. Lee, W-S. Liao. Efficient hydroxylation of $BaTiO_3$ nanoparticles by using hydrogen peroxide. Coll. Surf. A: Physicochem. Eng. Aspects 361 (2010) 143–149.

[29] T. Zhou, J-W. Zha, R-Y. Cui, B-H. Fan, J-K. Yuan, Z-M. Dang. Improving Dielectric Properties of $BaTiO_3$/Ferroelectric Polymer Composites by Employing Surface Hydroxylated $BaTiO_3$ Nanoparticles. ACS Appl. Mater. Interfaces 3 (2011) 2184–2188.

[30] V. S. Puli, R. Elupula, B. C. Riggs, S. M. Grayson, R. S. Katiyar, D. B. Chrisey. Surface modified $BaTiO_3$-polystyrene nanocomposites for energy storage. Int. J. Nanotechnol. 11 (2014) 910–920.

[31] C-C. Li, Y-C. Lee, Y-M. Cheng. Effects of Interactions Among $BaTiO_3$, PVA, and B_2O_3 on the Rheology of Aqueous $BaTiO_3$ Suspensions. J. Am. Ceram. Soc. 93 (2010) 3049–3051.

[32] H. Ishii, K. Sugiyama, E. Ito, K. Seki. Energy Level Alignment and Interfacial Electronic Structures at Organic/Metal and Organic/Organic Interfaces. Adv. Mater. 11 (1999) 605−625.

[33] M. Zhu, X. Huang, K. Yang, X. Zhai, J. Zhang, J. He, P. Jiang. Energy Storage in Ferroelectric Polymer Nanocomposites Filled with Core−Shell Structured Polymer@$BaTiO_3$ Nanoparticles: Understanding the Role of Polymer Shells in the Interfacial Regions. ACS Appl. Mater. Interfaces 6 (2014) 19644−19654.

[34] ASTM D3616–95. Standard Test Method for Rubber. Determination of Gel, Swelling Index, and Dilute Solution Viscosity (2014).

[35] ASTM D120-14a. Standard Specification for Rubber Insulating Gloves. ASTM, West Conshohocken, PA, PA, pp. 1–9, (2014).

[36] IEC, "IEC 60903:2014. Live working - Electrical insulating gloves." IEC, p. 117, 2014.

[37] N. González, J-R. Riba, M. A. Custal, E. Armelin. Improvement of Insulation Effectiveness of Natural Rubber by Adding Hydroxyl-Functionalized Barium Titanate Nanoparticles. IEEE Trans. Dielectr. Electr. Insul, 24 (6), 2017.

[38] H.A. Al-Abadleh, H.A. Al-Hosney, V.H. Grassian. The importance of water in surface composition and surface reactivity, J. Mol. Catal. A: Chem. 228 (2005) 47–54.

[39] S. Luo, S. Yu, R. Sun, C-P. Wong. Nano Ag-Deposited $BaTiO_3$ Hybrid Particles as Fillers for Polymeric Dielectric Composites: Toward High Dielectric Constant and Suppressed Loss. ACS Appl. Mater. Interfaces 6 (2014) 176−182.

[40] M. Huang, L. B. Tunnicliffe, A. G. Thomas, J. J.C. Busfield, The glass transition, segmental relaxations and viscoelastic behaviour of particulate-reinforced natural rubber. Eur. Polym. J. 67 (2015) 232–241.

[41] Prateek, V. K. Thakur, R. K. Gupta. Recent Progress on Ferroelectric Polymer-Based Nanocomposites for High Energy Density Capacitors: Synthesis, Dielectric Properties, and Future Aspects. Chem. Rev. 116 (2016) 4260−4317.

[42] Q. Chen, R.Y. Hong, W.G. Feng. Preparation and characterization of composites from $Ba_{0.7}Sr_{0.3}TiO_3$ and polystyrene. J. Alloys Comp. 609 (2014) 274–283.

[43] M. Hernández, J. L. Valentín, M. A. López-Manchado, T. A. Ezquerra, Influence of the vulcanization system on the dynamics and structure of natural rubber: Comparative study by

means of broadband dielectric spectroscopy and solid-state NMR spectroscopy. Eur. Polym. J. 68 (2015) 90–103.

[44] J. Carretero-González, T.A. Ezquerra, S. Amnuaypornsri, S. Toki, R. Verdejo, A. Sanz, J. Sakdapipanich, B. S. Hsiao, M.A. López-Manchado. Molecular dynamics of natural rubber as revealed by dielectric spectroscopy: The role of natural cross–linking. Soft Matter 6 (2010) 3636–3642.

[45] H. Kargarzadeh, I. Ahmad, I. Abdullah, R. Thomas, A. Dufresne, S. Thomas, A. Hassan. Functionalized Liquid Natural Rubber and Liquid Epoxidized Natural Rubber: A Promising Green Toughening Agent for Polyester. J. Appl. Polym. Sci. 132 (2015), 41292–41307.

[46] H.M. Jung, J.H. Kang, S.Y. Yang, J.C. Won, Y.S. Kim, Barium titanate nanoparticles with diblock copolymer shielding layers for high-energy density nanocomposites, Chem.Mater. 22 (2010) 450-456.

[47] H. Luo, D. Zhang, C. Jiang, X. Yuan, C. Chen, K. Zhou, Improved dielectric properties and energy storage density of poly(vinylidene fluoride-co-hexafluoropropylene) nanocomposite with hydantoin epoxy resin coated $BaTiO_3$, ACS Appl. Mater. Interfaces 7 (2015) 8061-8069.

[48] M. Rahimabady, M.S. Mirshekarloo, K. Yao, L. Lu, Dielectric behaviors and high energy storage density of nanocomposites with core-shell $BaTiO_3$@TiO_2 in poly(vinylidene fluoride-hexafluoropropylene), Phys. Chem. Chem. Phys. 15 (2013) 16242−16248.

[49] Y.Y. Sun, Z.Q. Zhang, C.P. Wong, Influence of interphase and moisture on the dielectric spectroscopy of epoxy/silica composites, Polymer 46 (2005) 2297-2305.

[50] F. Kremer, A. Schönhals (*Eds.*). *Broadband Dielectric Spectroscopy*, F. Kremer, A. Schönhals, Springer-Verlag Berlin Heidelberg, 2003

[51] D. Boese, F. Kremer, Molecular Dynamics in Bulk cis-Polyisoprene as Studied by Dielectric Spectroscopy. Macromolecules 23 (1990) 829–835.

[52] K. Adachi, T. Kotaka, Dielectric Normal Mode Relaxation. Prog. Polym. Sci. 18 (1993) 585-622.

[53] N. Xu, L. Hu, Q. Zhang, X. Xiao, H. Yang, E. Yu. Significantly Enhanced Dielectric Performance of Poly(vinylidene fluoride-*co*-hexafluoropylene)-based Composites Filled with Hierarchical Flower-like TiO_2 Particles. ACS Appl. Mater. Interfaces, 7 (2015) 27373−27381.

[54] Q. Huang, H. Luo, C. Chen, X. Zhou, K. Zhou, D. Zhang, Enhanced energy density in P(VDF-HFP) nanocomposites with gradient dielectric fillers and interfacial polarization. J. Alloys Comp. 696 (2017) 1220−1227.

[55] G. M. Tsangaris, G. C. Psarras, N. Kouloumbi, Electric modulus and interfacial polarization in composite polymeric systems, J. Mater Sci. 33 (1998) 2027−2037.

[56] X. Y. Huang, L. Y. Xie, Z. W. Hu, P. K. Jiang, Influence of $BaTiO_3$ Nanoparticles on Dielectric, Thermophysical and Mechanical Properties of Ethylene-Vinyl Acetate Elastomer/$BaTiO_3$ Microcomposites. IEEE Trans. Dielectr. Electr. Insul. 2011, 18, 375−383.

[57] K. Yu, Y. Niu, F. Xiang, Y. Zhou, Y. Bai, H. Wang. Enhanced electric breakdown strength and high energy density of barium titanate filled polymer nanocomposites. J. Appl. Phys. 114 (2013) 174107−174107.

Table 1. Compounding formulation used to prepare NR/$BaTiO_3$-OH nanocomposites (in phr).[a)]

Reagents	**NR**	**$BaTiO_3$-OH 0.25 phr**	**$BaTiO_3$-OH 0.50 phr**	**$BaTiO_3$-OH 1.0 phr**	**$BaTiO_3$-OH 5.0 phr**	**$BaTiO_3$-OH 10.0 phr**
Latex	100	100	100	100	100	100
Accelerator	6.0	6.0	6.0	6.0	6.0	6.0
Sulphur	6.0	6.0	6.0	6.0	6.0	6.0
Antioxidant	8.0	8.0	8.0	8.0	8.0	8.0
ZnO	8.0	8.0	8.0	8.0	8.0	8.0
TiO_2	5.0	4.75	4.5	4.0	0.0	0.0
$BaTiO_3$-OH	-	0.25	0.50	1.0	5.0	10.0
Other fillers	7.0	7.0	7.0	7.0	7.0	7.0

[a)] phr = parts per hundred of rubber per weight.

Table 2. Thermal properties for vulcanized rubber films modified with $BaTiO_3$-OH nanoparticles.

Sample	Ceramic content phr	T_g [a] (ºC)	$T_{d,max}$ [b] (ºC)	Char yield (wt. %)
Pristine NR	0.00	-64.1	374	1.8
NR/$BaTiO_3$-OH	0.25	-60.2	376	1.5
NR/$BaTiO_3$-OH	0.50	-60.6	378	2.0
NR/$BaTiO_3$-OH	1.00	-62.7	381	2.5
NR/$BaTiO_3$-OH	5.00	-63.5	381	5.7
NR/$BaTiO_3$-OH	10.0	-64.0	381	10.0

[a] Glass transition temperature obtained by DSC in the second scan, after dynamic curing at 20 ºC/min, [b] Temperature of the maximum decomposition rate based on the TGA data at 10 ºC/min.

FIGURE CAPTIONS

Figure 1. (a) Infrared spectrum with the absorption bands comparison between films prepared without $BaTiO_3$-OH particles and composites with 0.25 phr and 10 phr of ceramic compound. (b) Magnification of the 1450-1600 cm^{-1} and 900-1200 cm^{-1} zones showing an increase of CO_3^{2-} and –OH absorption bands.

Figure 2. XRD patterns of: $BaTiO_3$-OH ceramic particles, the vulcanized NR film without perovskite, and the NR/$BaTiO_3$-OH films with several weight fractions of ceramic filler.

Figure 3. (a) DSC thermograms of the second heating scan after dynamic curing at 20 ºC/min and (b) Thermogravimetric curves at 10 ºC/min in N_2 atmosphere for NR vulcanized films. The inset represents the char yield at 600 ºC.

Figure 4. SEM micrographs with low (left) and high (right) magnifications of the cross-section from NR vulcanized films: (a, b) pristine vulcanized NR; (c,d) NR/$BaTiO_3$-OH 0.25 phr; (e,f) NR/$BaTiO_3$-OH 0.5 phr; (g,h) NR/$BaTiO_3$-OH 1.0 phr; (i,j) NR/$BaTiO_3$-OH 5.0 phr; (k,l) NR/$BaTiO_3$-OH 10 phr. (m) EDX analysis from sample NR/$BaTiO_3$-OH 10 phr.

Figure 5. Dependence of the tensile strength and elongation at break of pristine NR and NR/$BaTiO_3$-OH composites loaded with perovskite particles.

Figure 6. (a) Real and (b) imaginary part of the dielectric permittivity for all systems as a function of frequency, at 253.15 K (-20ºC).

Figure 7. (a) Real part of the dielectric permittivity and (b) imaginary part of electric modulus, as a function of temperature at 0.1 Hz, for all studied systems. Inset presents the variation of imaginary part of the electric modulus versus frequency, at 423.15 K (150 ºC), for all systems.

Figure 8. Comparison of the NR characteristic breakdown strength (E_B), normalized with the film thickness, as a function of $BaTiO_3$ content (surface-functionalized and non-functionalized). NR/$BaTiO_3$ E_B results were taken from previous work [12].

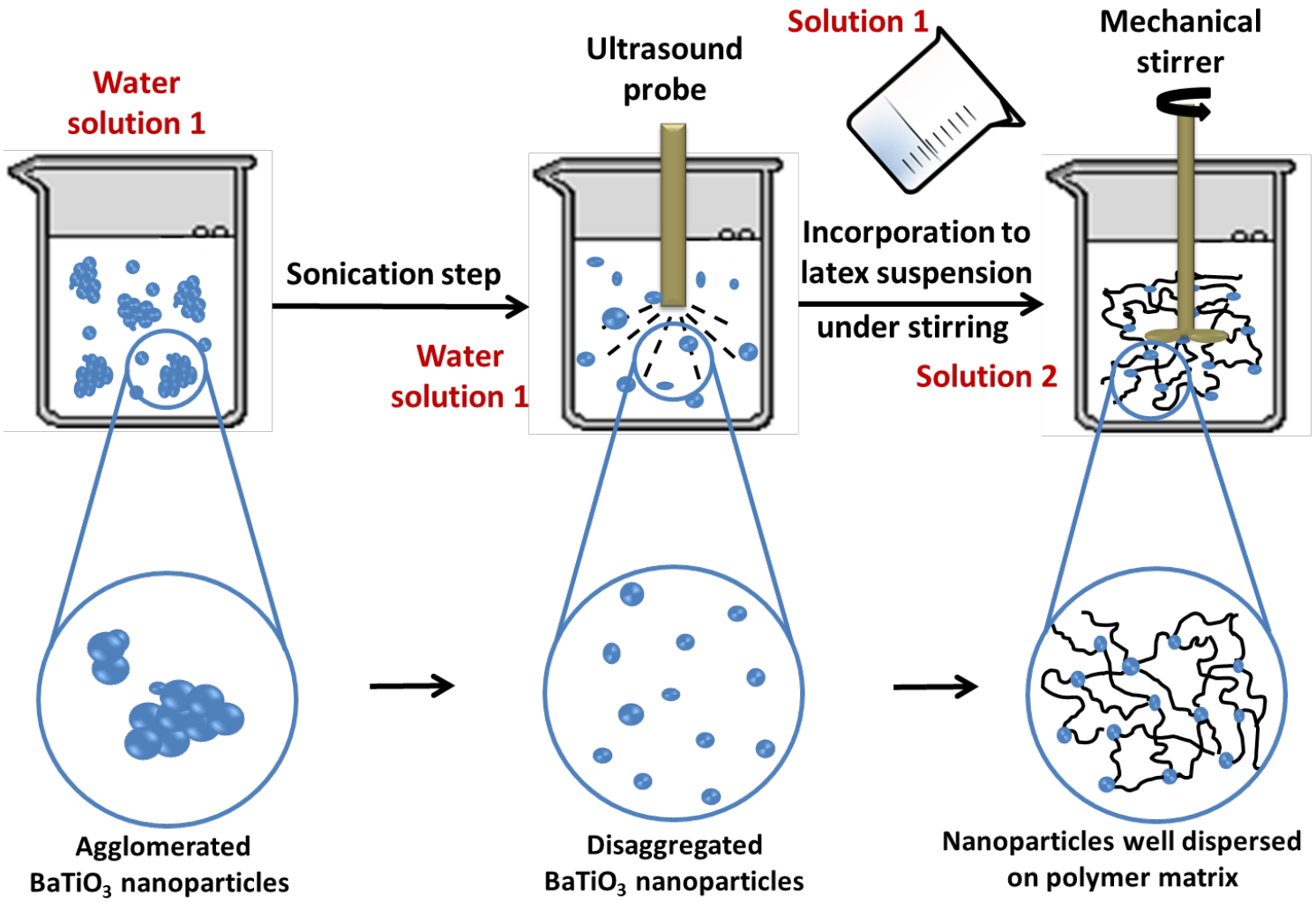

Scheme 1. Illustration of sonication process of $BaTiO_3$ solid particles and its incorporation in the latex suspension.

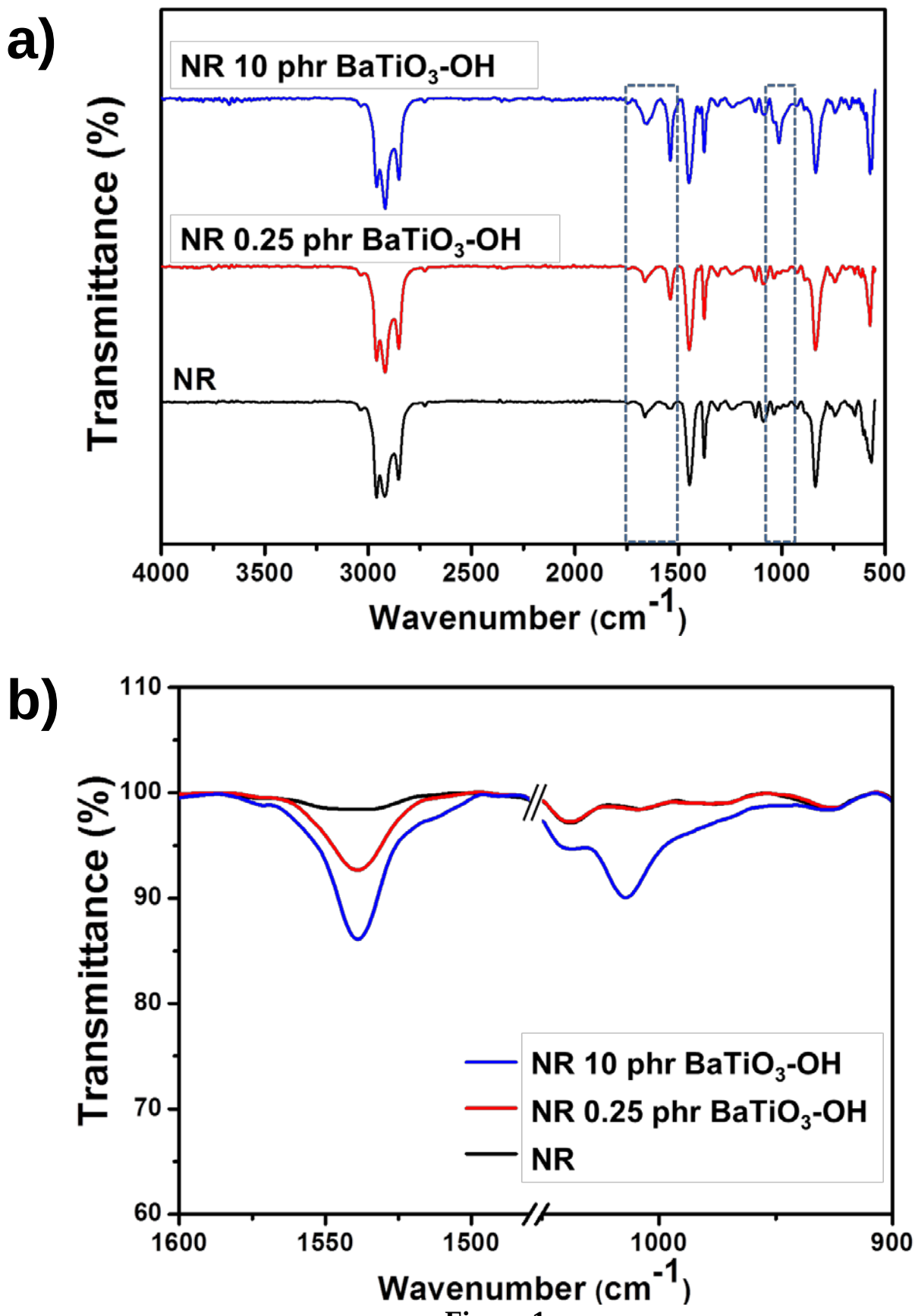
a)
NR 10 phr BaTiO3-OH
NR 0.25 phr BaTiO3-OH
NR
Transmittance (%)
4000
3500
3000
2500
2000
1500
1000
500
Wavenumber (cm-1)
b)
110
100
90
80
70
60
Transmittance (%)
1600
1550
1500
1000
900
Wavenumber (cm-1)
NR 10 phr BaTiO3-OH
NR 0.25 phr BaTiO3-OH
NR

Figure 1

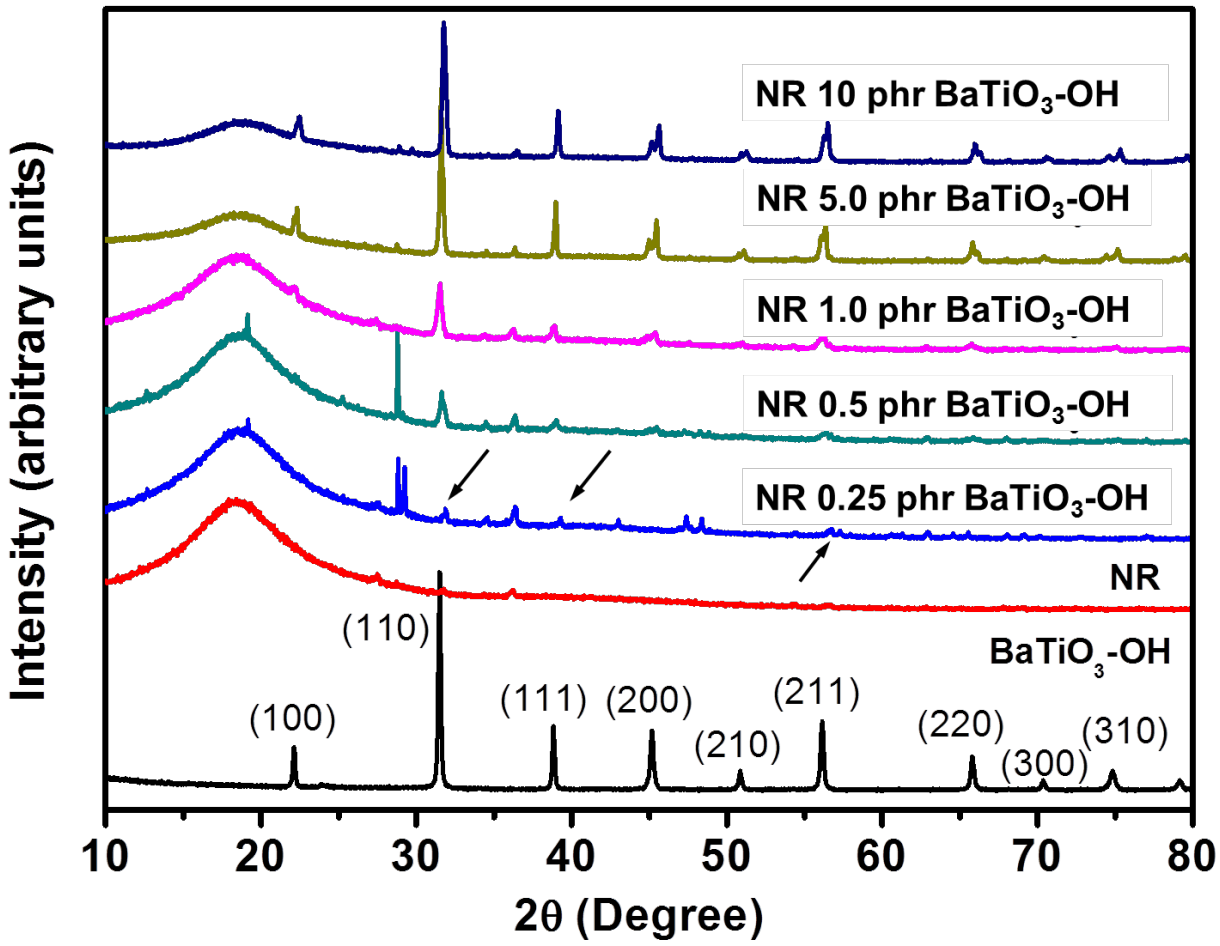
NR 10 phr BaTiO3-OH
NR 5.0 phr BaTiO3-OH
NR 1.0 phr BaTiO3-OH
NR 0.5 phr BaTiO3-OH
NR 0.25 phr BaTiO3-OH
NR
BaTiO3-OH
(100)
(110)
(111)
(200)
(210)
(211)
(220)
(300)
(310)
Intensity (arbitrary units)
2θ (Degree)
10
20
30
40
50
60
70
80

Figure 2

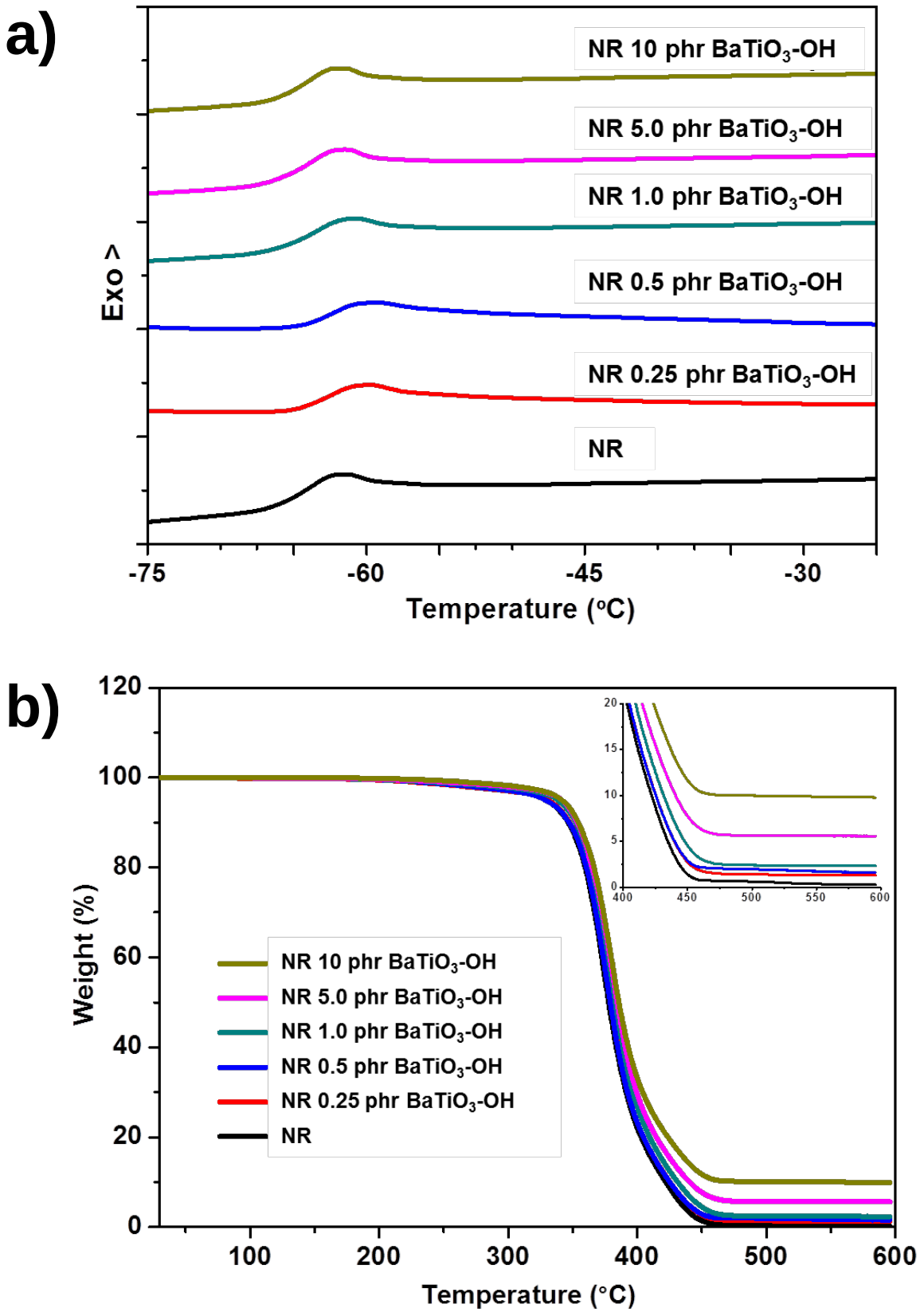
a)
NR 10 phr BaTiO3-OH
NR 5.0 phr BaTiO3-OH
NR 1.0 phr BaTiO3-OH
NR 0.5 phr BaTiO3-OH
NR 0.25 phr BaTiO3-OH
NR
Exo >
-75
-60
-45
-30
Temperature (°C)
b)
120
100
80
60
40
20
0
Weight (%)
NR 10 phr BaTiO3-OH
NR 5.0 phr BaTiO3-OH
NR 1.0 phr BaTiO3-OH
NR 0.5 phr BaTiO3-OH
NR 0.25 phr BaTiO3-OH
NR
100
200
300
400
500
600
Temperature (°C)

Figure 3

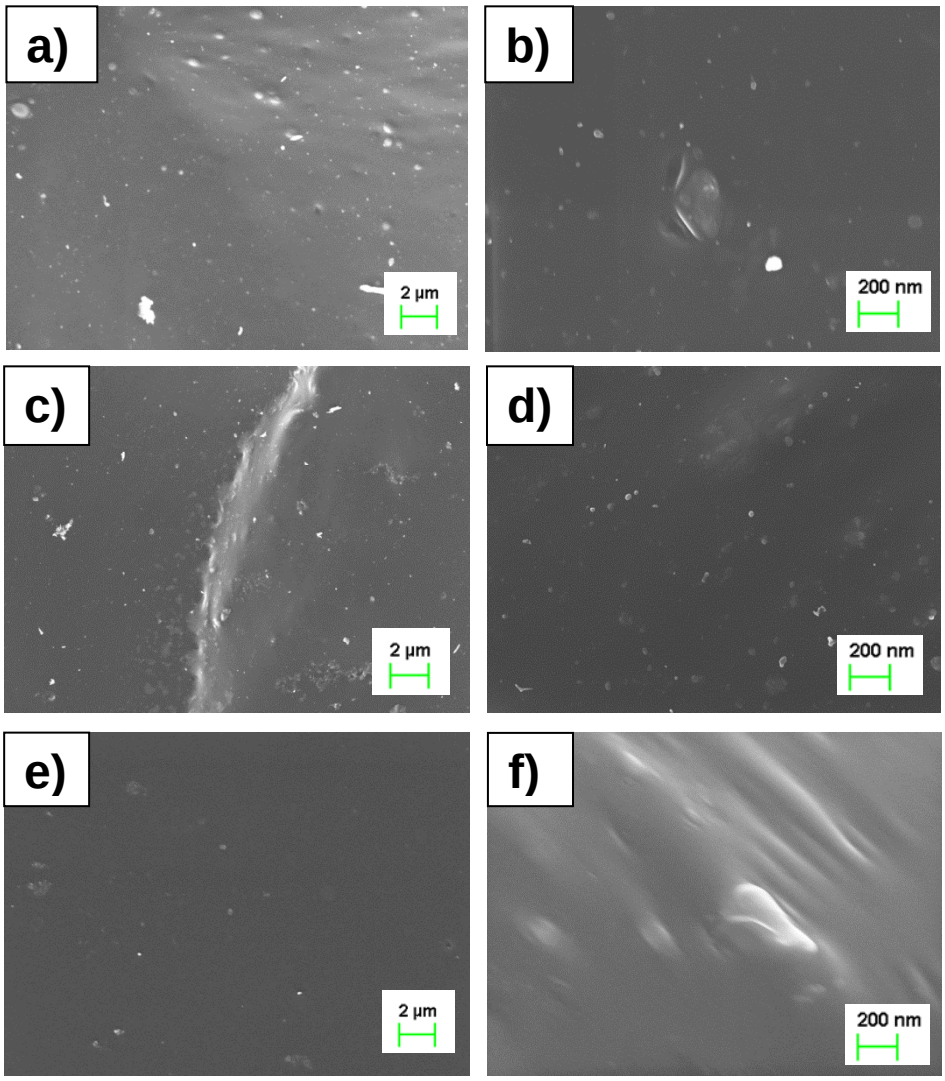

Figure 4

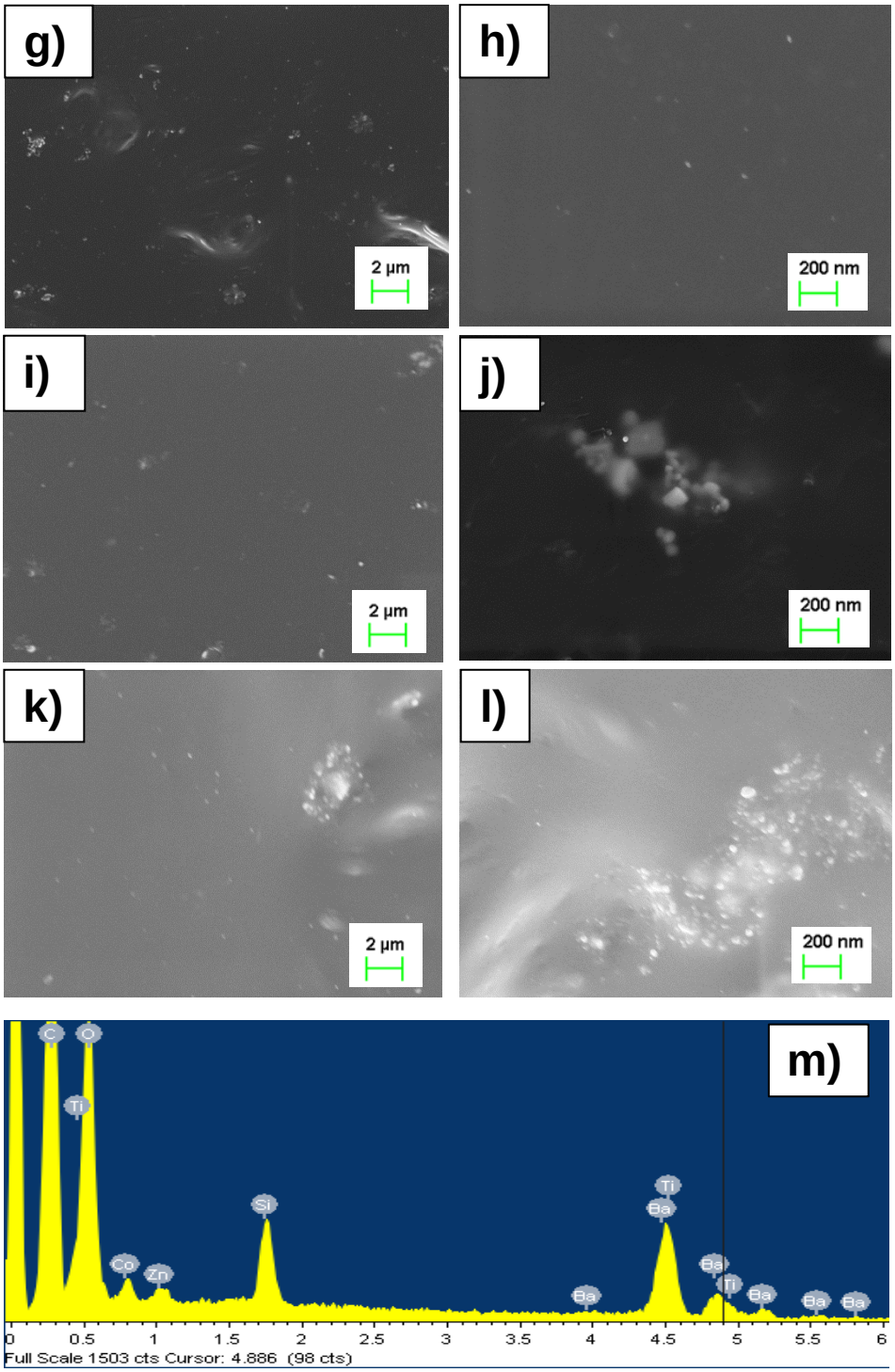

Figure 4 (continuation…)

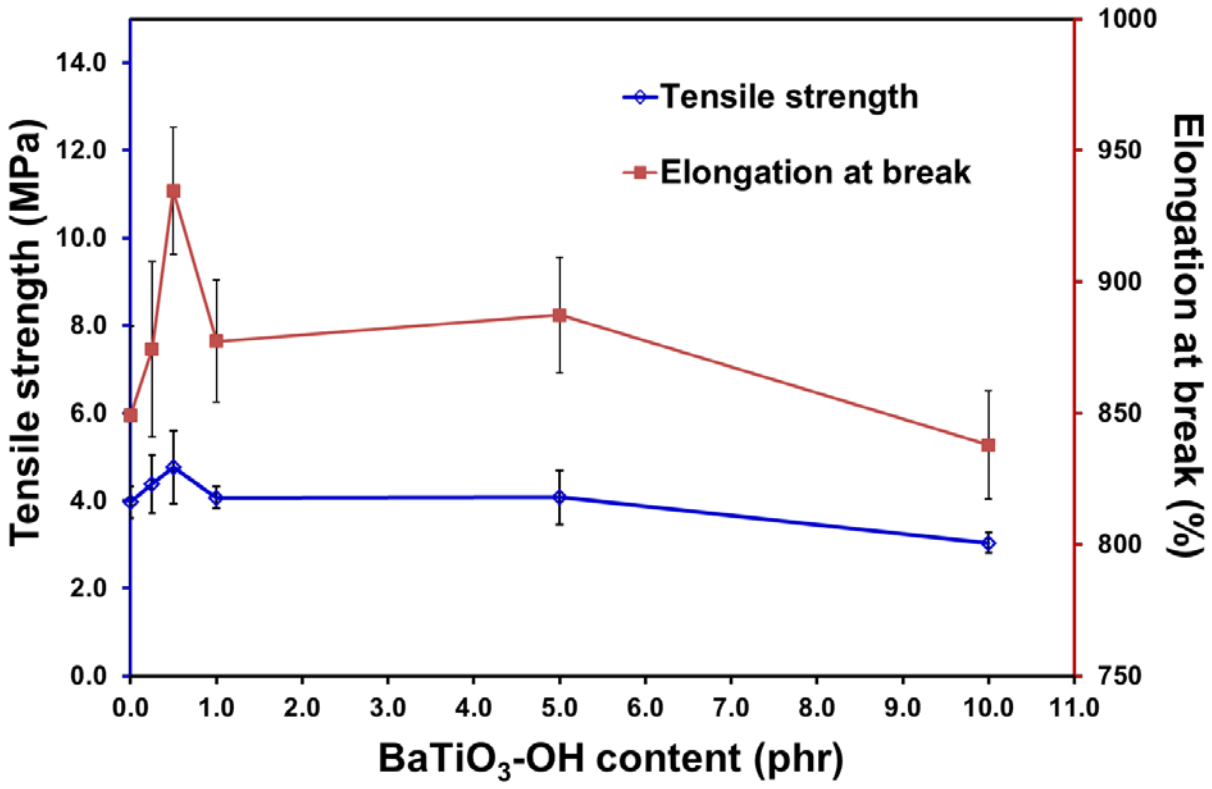
Tensile strength
Elongation at break
Tensile strength (MPa)
Elongation at break (%)
BaTiO3-OH content (phr)
0.0
2.0
4.0
6.0
8.0
10.0
12.0
14.0
750
800
850
900
950
1000
0.0
1.0
2.0
3.0
4.0
5.0
6.0
7.0
8.0
9.0
10.0
11.0

Figure 5

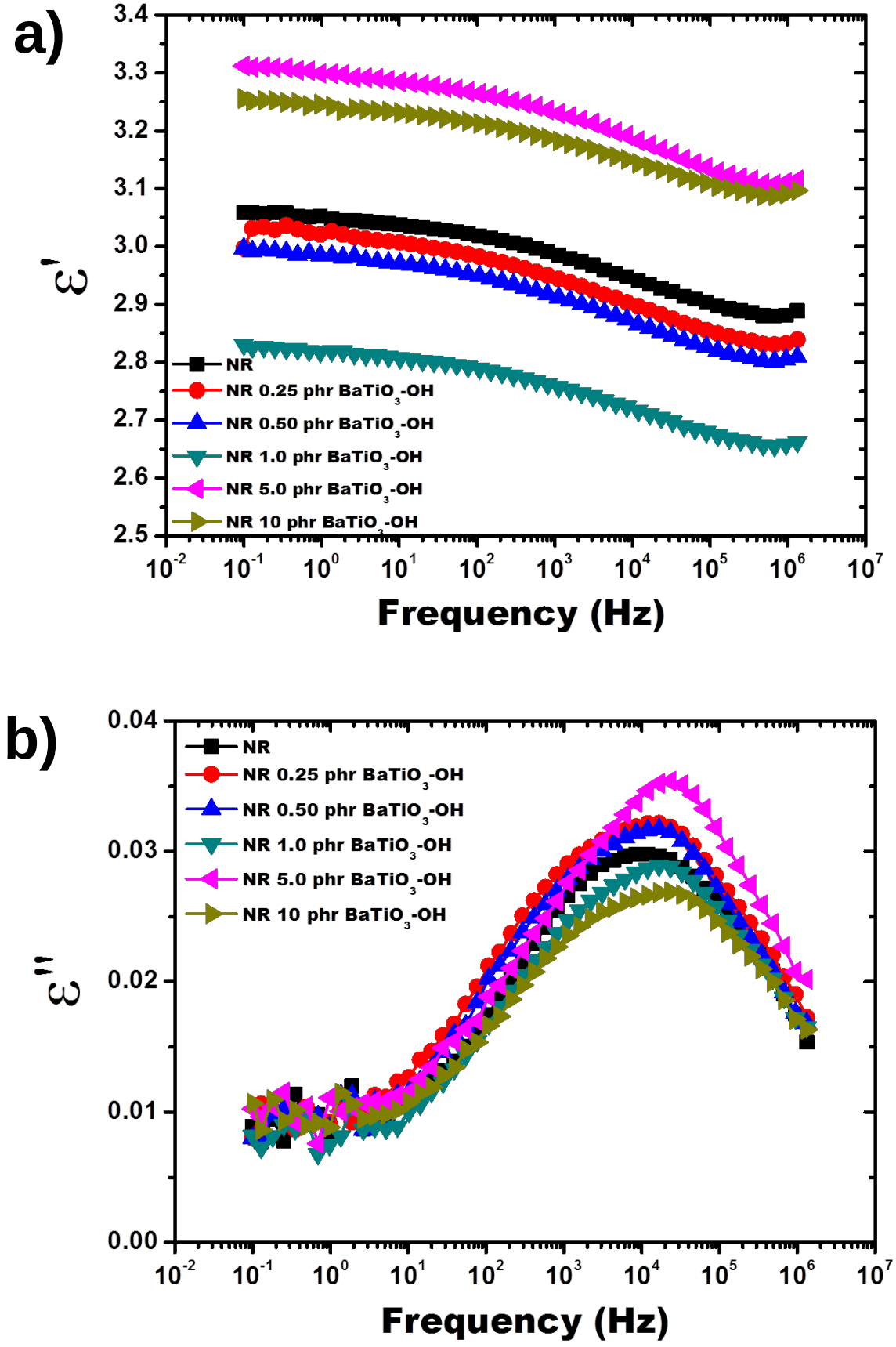
a)
3.4
3.3
3.2
3.1
3.0
2.9
2.8
2.7
2.6
2.5
ε'
NR
NR 0.25 phr BaTiO3-OH
NR 0.50 phr BaTiO3-OH
NR 1.0 phr BaTiO3-OH
NR 5.0 phr BaTiO3-OH
NR 10 phr BaTiO3-OH
10-2 10-1 100 101 102 103 104 105 106 107
Frequency (Hz)
b)
0.04
0.03
0.02
0.01
0.00
ε''
NR
NR 0.25 phr BaTiO3-OH
NR 0.50 phr BaTiO3-OH
NR 1.0 phr BaTiO3-OH
NR 5.0 phr BaTiO3-OH
NR 10 phr BaTiO3-OH
10-2 10-1 100 101 102 103 104 105 106 107
Frequency (Hz)

Figure 6

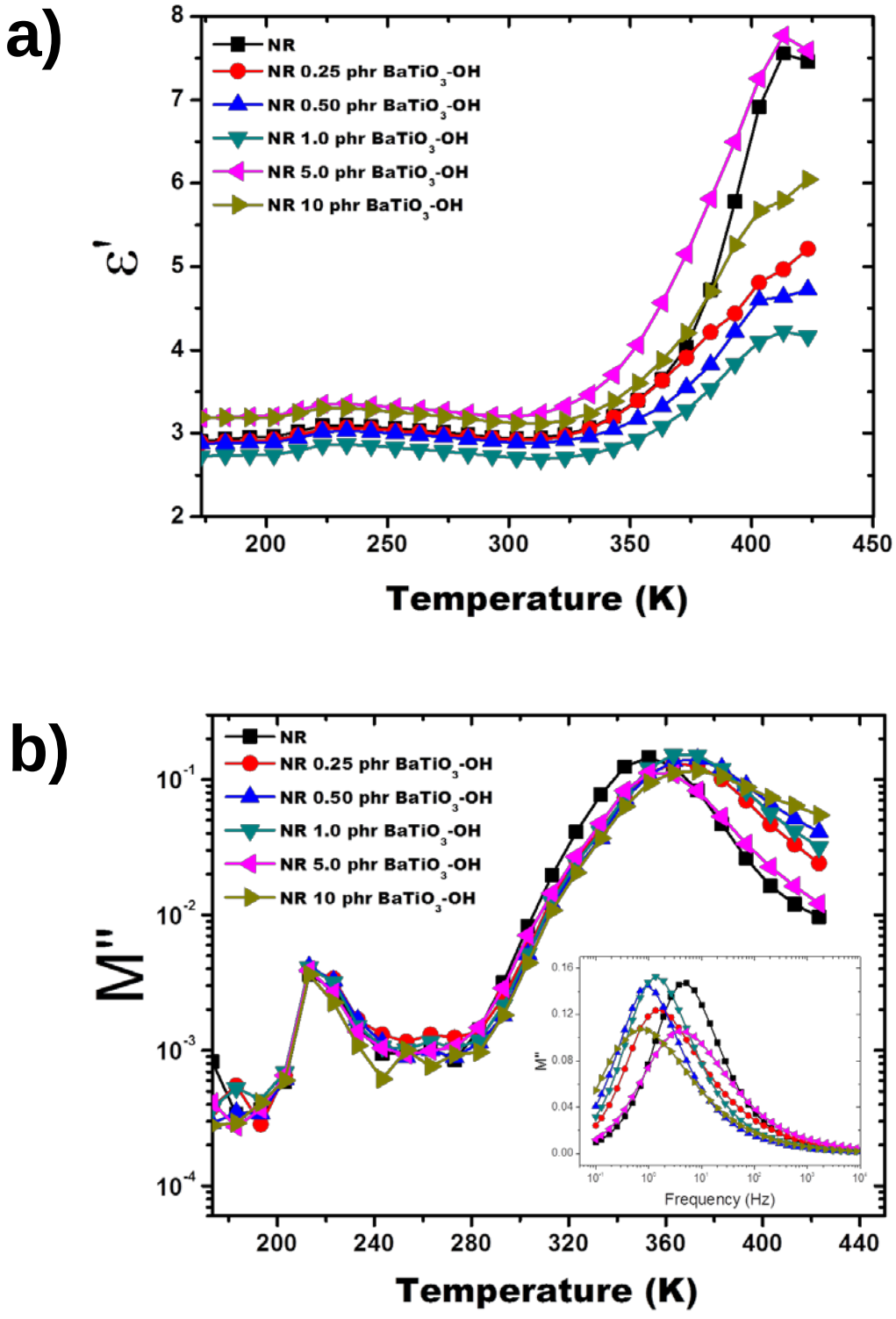
a)
NR
NR 0.25 phr BaTiO3-OH
NR 0.50 phr BaTiO3-OH
NR 1.0 phr BaTiO3-OH
NR 5.0 phr BaTiO3-OH
NR 10 phr BaTiO3-OH
ε'
Temperature (K)
b)
M''
Frequency (Hz)

Figure 7

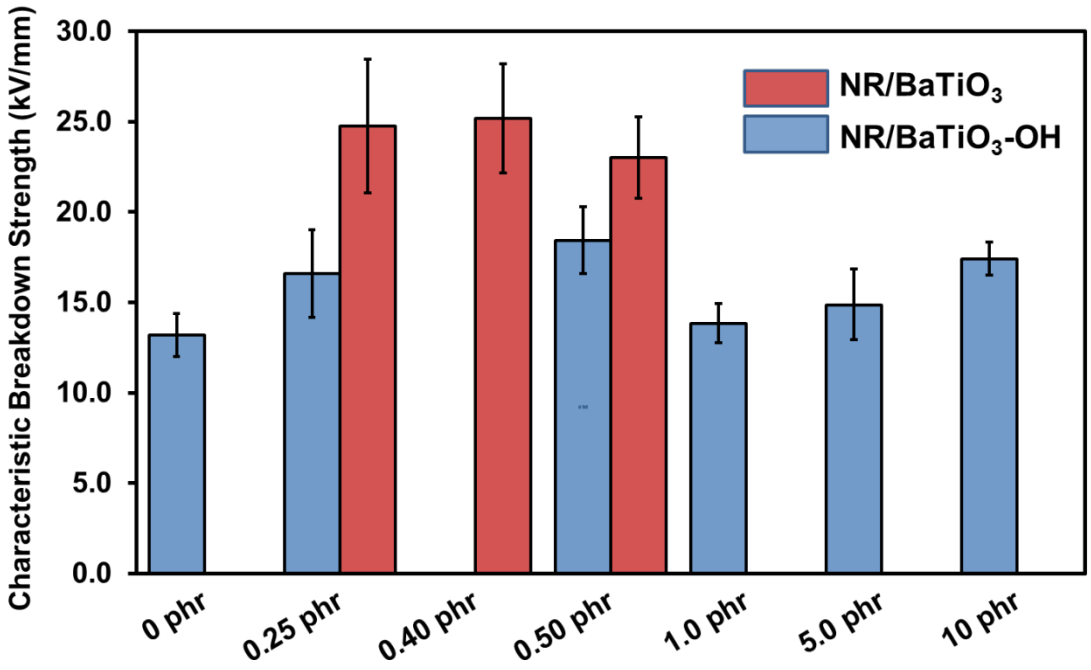
Characteristic Breakdown Strength (kV/mm)
30.0
25.0
20.0
15.0
10.0
5.0
0.0
NR/BaTiO3
NR/BaTiO3-OH
0 phr
0.25 phr
0.40 phr
0.50 phr
1.0 phr
5.0 phr
10 phr

Figure 8